Synthetic and Systems Biotechnology 10 (2025) 897–906

Contents lists available at ScienceDirect

Synthetic and Systems Biotechnology

journal homepage: www.keaipublishing.com/en/journals/synthetic-and-systems-biotechnology

Original Research Article

Extending dynamic and operational range of the biosensor responding to L-carnitine by directed evolution

Tingting Li [a,b,1], Huina Dong [b,c,*,1], Jinlong Li [b,1], Huiying Wang [b], Chunxiang Pu [b], Siyu Chen [b], Zhiying Yang [b], Xinyi Ren [b], Xuan Liu [b], Zhaoxia Jin [a,**], Dawei Zhang [a,b,c,d,***]

[a] School of Biological Engineering, Dalian Polytechnic University, Dalian, China
[b] Tianjin Institute of Industrial Biotechnology, Chinese Academy of Sciences, Tianjin, China
[c] University of Chinese Academy of Sciences, Beijing, China
[d] State Key Laboratory of Engineering Biology for Low-Carbon Manufacturing, China

ARTICLE INFO

Keywords:
Transcription factor
CaiF
Detection range
Biosensor
L-carnitine

ABSTRACT

L-carnitine is a quaternary amine compound essential for eukaryotic metabolism. It is mainly involved in the oxidative decomposition of medium-and long-chain fatty acids and provides energy for the body. Therefore, it is widely used in health care and food additives. As a pivotal transcriptional activator of L-carnitine metabolism, CaiF is notably activated by crotonobetainyl-CoA, a key intermediate product in the carnitine metabolic pathway. Capitalizing on this mechanism, a sophisticated biosensor was ingeniously developed. Nevertheless, it is worth mentioning that the biosensor currently exhibits a relatively restricted detection range, which results in some specific limitations in practical application scenarios. In this paper, we constructed a biosensor based on CaiF and developed a strategy for modifying this biosensor. The structural configuration of CaiF was formulated by computer-aided design, and the DNA binding site was simulated, which was verified by alanine scanning. Functional Diversity-Oriented Volume-Conservative Substitution Strategy of the key sites of CaiF was conducted to extend the dynamic range of the biosensor. The biosensor based on CaiF$^{Y47W/R89A}$, which exhibited a considerably expanded concentration response range, from 10^{-4} mM–10 mM, was obtained. The response range was 1000-fold wider and the output signal intensity was 3.3-fold higher to that of the control biosensor. These variants may have great value in improving the L-carnitine production process.

1. Introduction

L-carnitine, also known as vitamin BT, is a generally recognized as safe (GRAS) state vitamin-like molecule that plays a crucial role in eukaryotes by helping to transport medium and long-chain fatty acids, and transferring activated acyl residues across the cell membrane [1,2]. Humans and animals mainly obtain L-carnitine through diet [3,4]. L-carnitine deficiency can cause problems such as energy metabolism disorders and impaired cell membrane function. Therefore, L-carnitine and its derivatives can be used in many medical fields, including the treatment of cardiovascular diseases and as nutritional supplements to enhance training efficiency and weight control [5,6].

The conventional production of L-carnitine predominantly relies on chemical synthesis methodologies or direct extraction from biological sources, processes that are characterized by technical complexity and significant economic expenditures. Consequently, the biosynthesis of L-carnitine by *Escherichia coli* has important research value and application prospect [7]. The genes involved in L-carnitine metabolism of *E. coli* comprise two divergent *caiTABCDEF* and *fixABCX* operons, which are induced either by L-carnitine or crotonobetaine under anaerobic conditions [8,9]. This regulation is activated by both cyclic adenosine monophosphate receptor protein (CRP) and CaiF, a specific transcriptional activator of carnitine metabolism in *E. coli* [8]. As a co-activator of CaiF, crotonobetainyl-CoA can be obtained by two-step enzymatic

Peer review under the responsibility of Editorial Board of Synthetic and Systems Biotechnology.
* Corresponding author. Tianjin Institute of Industrial Biotechnology, Chinese Academy of Sciences, Tianjin, China.
** Corresponding author.
*** Corresponding author. Tianjin Institute of Industrial Biotechnology, Chinese Academy of Sciences, Tianjin, China.
E-mail addresses: dong_hn@tib.cas.cn (H. Dong), jinzx2018@163.com (Z. Jin), zhang_dw@tib.cas.cn (D. Zhang).
[1] These authors equally contributed to this work.

https://doi.org/10.1016/j.synbio.2025.04.012
Received 18 February 2025; Received in revised form 16 April 2025; Accepted 21 April 2025
Available online 22 April 2025

reaction with L-carnitine as substrate in *E. coli*. Firstly, under the action of CaiC (betaine: CoA ligase), L-carnitine connects with CoA to form carnitinyl-CoA, this step requires CaiT (carnitine: γ-butyrobetaine antiporter) to transport L-carnitine into the cell. Then, CaiD (carnitinyl-CoA dehydratase) dehydrates carnitinyl-CoA to form crotonobetainyl-CoA. CaiF can bind to crotonobetainyl-CoA, thereby activating the *fix* promoter [9–11]. Based on this theoretical foundation, a biosensor was successfully developed that responds in a dose-dependent manner to external L-carnitine was developed [12]. However, the dynamic range of this biosensor is about 10^{-4} mM–10^{-1} mM, which may be not sufficient to screen for the improved enzyme performance in a newly discovered or an engineered enzyme pool.

The use of biosensors for high-throughput screening is of great significance and significant advantages for finding a strain with high yield of L-carnitine [7]. However, most biosensors based on transcription factors often face challenges such as a narrow response range, insufficient stability, and lack of specificity, which collectively limit their application and further development. Therefore, to design and optimize transcription factor-based biosensors, researchers have developed a variety of strategies. One of these strategies is promoter engineering, which optimizes the core and operator regions of the promoter by designing different mutants. This process helps regulate the binding affinity of transcription factors, thereby improving the transcription efficiency of the reporter gene [13–16]. While promoter engineering represents a promising strategy for optimizing the performance characteristics of biosensors, detecting low-concentration target molecules may require other means to adjust the detection range and substrate specificity [17]. This need, in turn, limits the further improvement of biosensor performance. Therefore, constructing a unique genetic circuit that incorporates a cascade amplifier circuit is particularly important for detecting low-concentration effectors. By amplifying the signal in a step-by-step manner and reducing background noise, the detection sensitivity of the biosensor to low-concentration target molecules can be significantly enhanced [18–20]. Computer-aided design (CAD) optimization of transcription factors offers a more efficient and accurate modification strategy. By precisely designing and optimizing the ligand-binding domain (LBD) and DNA-binding domain (DBD) of transcription factors, it becomes more effective in accurately identifying and binding to specific ligands and DNA sequences, thereby enhancing the specificity and sensitivity of biosensors [21–23]. The comprehensive application of these strategies endows transcription factor-based biosensors with broad application prospects in high-throughput screening and dynamic regulation of metabolic pathways.

In this study, to enhance the detection range and output signal intensity of the biosensor, we first employed AlphaFold3 to predict the three-dimensional structure of CaiF and simulate its DNA-binding conformation, which was subsequently validated through alanine scanning mutagenesis. Based on the alanine scanning results, we performed site-directed mutagenesis on CaiF and further implemented combinatorial mutations by integrating effective single-point mutants with residues exhibiting significantly enhanced fluorescence signals in scanning assays. This rational engineering approach ultimately yielded an optimized biosensor mutant demonstrating a 1000-fold expanded detection range and 3.3-fold increased fluorescence signal output intensity compared to the original construct.

2. Materials and methods

2.1. Bacterial strains, plasmids and culture conditions

All of the strains and plasmids used in this study are listed in Table S1. *Escherichia coli* DH5α (Transgene, Beijing) was used for plasmid construction. *E. coli* was cultured in Luria-Bertani (LB) medium (10 g/L NaCl, 10 g/L tryptone and 5 g/L yeast extract) as well as 1.5 % agar for solid at 37 °C. Antibiotics were supplemented as follows: ampicillin (Ap, 100 μg/mL), apramycin (Apr, 50 μg/mL), kanamycin (Km, 50 μg/mL).

M9 minimal medium (6.78 g/L Na_2HPO_4, 3 g/L KH_2PO_4, 0.5 g/L NaCl, 1 g/L NH_4Cl, 1 mM $MgSO_4$, 0.1 mM $CaCl_2$, and 0.1 % (v/v) trace element solution, pH 7.0) with 24 g/L glycerol as the carbon source was used for the biosensor experiments. The trace element solution contained (in mg/L) $ZnSO_4{\cdot}7H_2O$ (10), $MnSO_4{\cdot}7H_2O$ (100), $FeSO_4{\cdot}7H_2O$ (100), $CuSO_4$ (2), and $NiCl_4{\cdot}6H_2O$ (0.2) and had pH ~1.0.

2.2. Construction of biosensor vectors

The plasmids used in this study are listed in Table S2. The Low-copy number vector pBBR was utilized as the backbone plasmid for L-carnitine biosensor construction [24,25]. All of the recombinant plasmids used in this study were constructed by Gibson assembly. Two L-carnitine biosensor plasmids, using *mCherry* or *sfGFP* as reporter gene, were successfully constructed. The process began with the amplification of the *fix* promoter from the *Escherichia coli* genome, which was then combined with the *sfGFP* gene segment using overlap-extension PCR and inserted into the pBBR vector, yielding the recombinant plasmid pBBR-*fix*-*sfGFP*. Then, the *caiF* gene was amplified from the *E. coli* genome and cloned into the recombinant plasmid, resulting in pBBR-*sfGFP*-*caiF*. Subsequently, the hom promoter from *Corynebacterium glutamicum* was introduced into the recombinant plasmid, creating the L-carnitine biosensor without the *caiC* segment, designated as pBBR-*sfGFP*-*caiF*. The final step involved amplifying the *caiC* segment from the *E. coli* genome and cloning it into the plasmid to generate the L-carnitine biosensor with sfGFP as the reporter gene, named pBBR-*sfGFP*-*caiF*-*caiC*. Notably, the B0015 double terminator was strategically placed between the *caiF* and *sfGFP* genes. To develop the L-carnitine biosensor with *mCherry* as the reporter gene, pBBR-*mCherry*-*caiF*-*caiC*, the existing *sfGFP* gene on the pBBR-*sfGFP*-*caiF*-*caiC* plasmid was replaced with *mCherry*.

2.3. Chassis cell construction

Genome editing of *E. coli* was based on the CRISPR/Cas9 method reported by Zhao et al. [26]. For example, the up- and downstream homologous arms of *caiA* were amplified, and fused by overlap-extension PCR, while the vector backbone was divided into two fragments with the N20 guide RNA sequence between them. Finally, the three resulting fragments were fused by Gibson Isothermal Assembly to create pCas9-Δ*caiA*, which was then introduced into host strain by chemical transformation, and a positive single colony was transferred to LB medium containing 10 mg/L arabinose and 100 μg/mL ampicillin, followed by cultivation at 30 °C for several generations to promote the integration of the construct into the genome. Then, colony PCR and Sanger sequencing with specific genomic primers were used to confirm that *caiA* was deleted successfully. Finally, the *caiA* deleted strain was transferred into LB medium and cultured at 37 °C to cure the pCas9 plasmid, resulting in the final strain. The other gene deletion strain was constructed using the same method.

2.4. Construction of l-carnitine biosensor mutants

The CaiF mutants were constructed by site-directed mutagenesis. The PCR reaction was conducted using the PrimerSTAR Max DNA polymerase (Takara, Japan) and the pBBR-*sfGFP* -*caiF*-*caiC* plasmids as the template DNA. The primers are listed in Supplementary Table S2. The PCR product was digested by *Dpn*I (Takara, Japan) at 37 °C for 1 h 30 min. Then it was transformed into competent cells of *E. coli* DH5α. After sequence verification, the extracted mutant plasmid was transferred into strain BW25113 (DE3) Δ*caiA* for expression using chemical transformation method.

2.5. Characterization of the l-carnitine biosensor

The biosensor was tested in BW25113 (DE3) Δ*caiA*. A single colony

was inoculated into LB and cultured overnight at 37 °C. Subsequently, inoculated into 0.8 mL of 96-well plates with fresh M9 medium containing Apr (50 μg/mL) at an initial OD_{600} of 0.05. L-carnitine (RiboBio, China) was added to the medium at different concentrations from 10^{-6} mM–10 mM, and the strains were subjected to fluorescence detection after incubation at 37 °C for 20 h. The fluorescence intensities and OD600 of the cells were measured by a Synergy Neo2 multimode microplate reader (BioTek, VT, USA). The wavelengths of excitation and emission for mCherry and sfGFP were 587/610 nm and 488/509 nm, respectively. By OD_{600} normalizing the fluorescence intensity, the specific fluorescence was estimated.

2.6. Molecule dynamic simulations

Structural prediction and modeling of the CaiF-DNA complex was performed using AlphaFold3 [27]. Following preparation, the 3D models of wild-type CaiF-DNA and CaiF-DNA (R75A) were employed as the initial complex for molecular dynamics (MD) simulations. Initially, the constructed model underwent energy minimization using AMBER22 [28], which was also utilized for the subsequent MD simulation of the final model, employing the ff14SB and gaff2 force field with the hydrogen mass repartitioning (HMR) method. After heating and equilibration, a 100 ns MD simulation was conducted without constraints. The complete simulation methodology employed in this study is available in the supporting information. The MD trajectories were collected for further analysis and identification of relevant binding poses.

2.7. Data analysis

All experiments were repeated three times, and the results were taken as the average value. Prism software was used for paired comparison using unpaired two-sided *t*-test for statistical analysis. The data in the graph showed a statistically significant difference (*$p < 0.05$; **$p < 0.01$; ***$p < 0.001$; ****$p < 0.0001$).

3. Results and discussion

3.1. Design of an in vivo activation l-carnitine biosensor

Based on the transcription factor CaiF, Pierre Kugler et al. [12] constructed a biosensor that can respond to different substrates in different *E. coli* chassis. The detection range of the biosensor is limited to 10^{-4} mM to 10^{-1} mM, which poses significant challenges for its applicability in genetic designs that require a broader dynamic range.

In order to improve the detection range of biosensors, a biosensor based on transcription factor CaiF was constructed. The sensor consists of three main parts: first, the transcription factor CaiF is regulated by L-carnitine metabolites; secondly, *caiC* and *caiF* are co-expressed, and the effectors in the L-carnitine metabolic pathway exist in the form of coenzyme A [12], which avoids the interference of endogenous metabolic pathways in host cells [9]; finally, a selectable marker gene or reporter gene was introduced for the characteristic analysis of biosensors. In this constructed genetic circuit, once the presence of crotonobetaine-CoA is detected, the CaiF protein is activated, thereby promoting the expression of the fluorescent reporter gene (Fig. 1).

In the sensor construction, we first screened the reporter genes, including mCherry, which is monomer derivatives of DsRed protein and suitable for long-term imaging, and Superfolder GFP (sfGFP) is an engineered variant of green fluorescent protein (GFP) that exhibits higher folding efficiency and photostability compared to wild-type GFP [29,30] (Fig. 2a). The presence of glucose will affect the expression of *cai* and *fix* operons, thus, glycerol was used as carbon source, which significantly increased the utility and sensitivity of the biosensor [12]. To evaluate the differential response of two distinct biosensors harboring different reporter genes to L-carnitine, varying concentrations of L-carnitine were introduced into the glycerol minimal M9 medium. The results indicated that the biosensor with mCherry did not show fluorescence signal in response to L-carnitine. In contrast, the biosensor with sfGFP displayed a dose-dependent fluorescence signal when exposed to L-carnitine (Fig. 2b). This may be due to mCherry's poor fluorescence intensity and long maturation time [31]. When exogenous low-concentration L-carnitine is added, mCherry's fluorescence signal change may be too subtle to be accurately detected [32]. Moreover, though mCherry has good photostability, its excited-state electrons easily react with oxygen, generating reactive oxygen species [31]. This makes its photobleaching tolerance weaker than that of sfGFP, which may further affect its long-term imaging performance. In contrast, sfGFP has advantages in fluorescence intensity and maturation time, making it more effective in emitting fluorescence signals under the same experimental conditions [32,33]. Consequently, in subsequent experiments, the sfGFP was utilized as the reporter for the biosensor.

In order to determine the response range of the biosensor with sfGFP to L-carnitine in the BW25113 (DE3) Δ*caiA*, the exogenous addition concentration range of L-carnitine was from 10^{-6} mM–10 mM. The biosensor exhibited a concentration-dependent fluorescence response within the L-carnitine concentration range of 10^{-4} mM to 10^{-2} mM. When the concentration reaches 10^{-2} mM, the fluorescence response tends to be saturated. Demonstrating saturation of the receptor-binding capacity in the detection system (Fig. 2c).

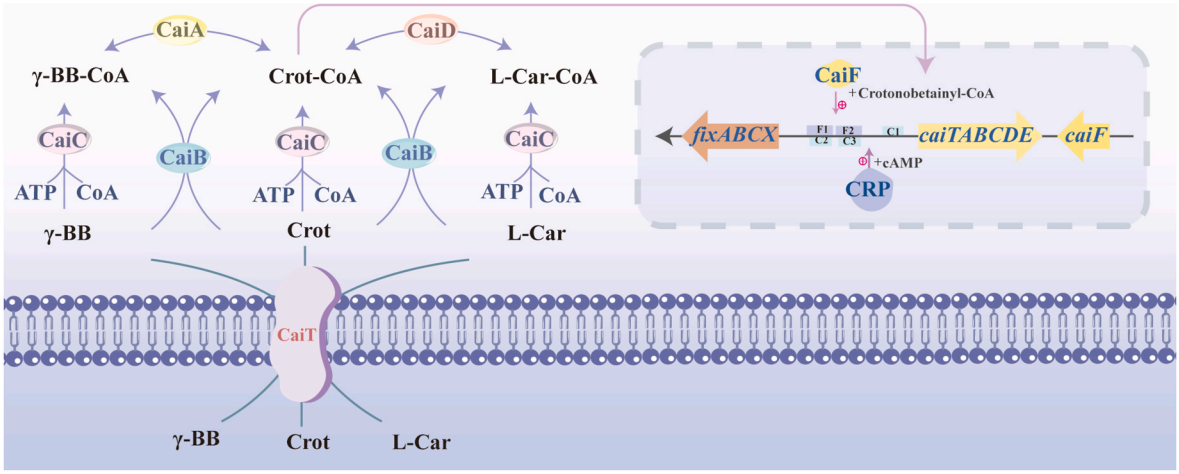

Fig. 1. Schematic of Endogenous Regulation of L-Carnitine in *Escherichia coli*. γ-BB, γ-butyrobetaine; l-car, L-Carnitine; Crot, crotonobetaine; γ-BB-CoA, γ-butyrobetainyl-CoA; l-car-CoA, l-carnitinyl-CoA; Crot-CoA, crotonobetainyl-CoA.

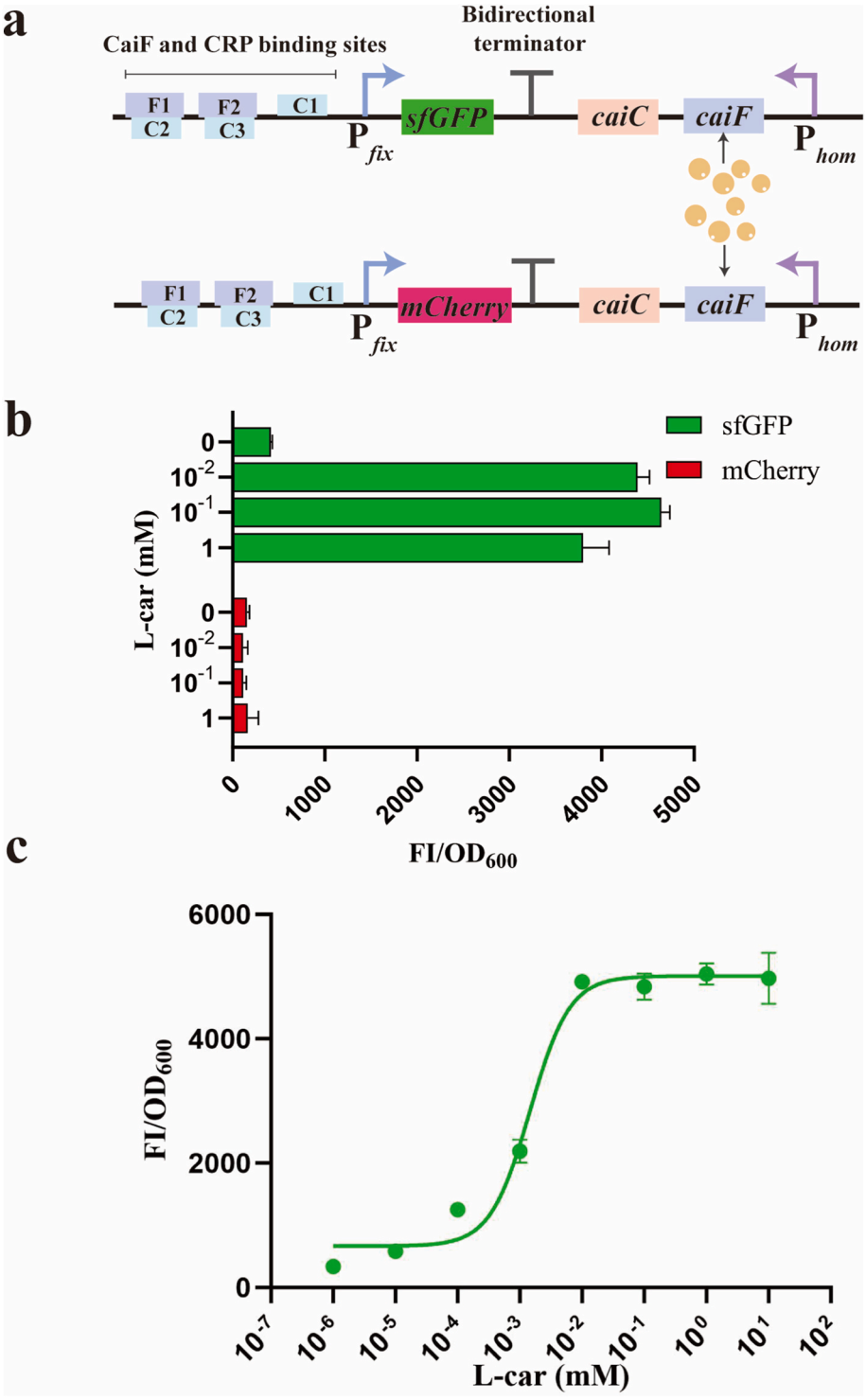

Fig. 2. A biosensor based on the transcription factor CaiF has been developed for the detection of L-carnitine. (a) The working principle of the biosensor. There are two reporter genes in the biosensor, *sfGFP* and *mCherry* (Down). (b) The biosensors corresponding to two different reporter genes were assessed using varying concentrations of L-carnitine. (c) Dose-response curves to exogenous L-carnitine for Sensor in BW25113 (DE3) Δ*caiA* cultivated in glycerol M9 medium. The fluorescence was determined at each indicated effector concentration and normalized to the cell density. The curves were fitted to the Hill equation. The maximum normalized fluorescence signal observed during the cultivation process is shown. Error bars indicate the standard deviation of the mean of three replicates.

3.2. Identification of the key binding sites of transcription factor CaiF

The interaction between transcription factors and DNA is a critical process in gene expression regulation, which largely depends on the precise recognition between specific amino acid residues and DNA molecules. CaiF (which Buchet et al. [9] speculate may function as a homodimer) can specifically bind to two sites (F1 and F2) in the *cai-fix* regulatory region. These sites contain 11 bp perfect inverted repeats separated by 13 base pairs between the two half-sites. The sequence is 5′-TTTCAATATTG-N13-CAATATTGAAA-3′ [8,9]. To elucidate the molecular mechanism of the CaiF transcriptional regulator, structural prediction and modeling of the CaiF-DNA complex were performed

using AlphaFold3 [27]. Structure analysis revealed several critical residues that directly interact with DNA (Fig. 3). These residues are predominantly located in the DNA-binding domain, establishing direct contacts with the DNA backbone and bases through hydrogen bonds and electrostatic interactions, which are essential for the specificity and functionality of the transcription factor. Based on these structural insights, alanine scanning mutagenesis was employed to systematically validate the function of these sites. This approach, involving the substitution of polar amino acids with the smaller alanine residue, enables the assessment of how alterations in charge distribution, stability, and thermodynamic properties affect substrate and DNA binging.

After excluding residues involved solely in main-chain interactions and hydrophobic contacts, 26 residues were selected for further validation (positions 11, 28, 38, 39, 40, 42, 43, 46, 47, 64, 69, 72, 74, 75, 89, 92, 93, 96, 97, 102, 103, 104, 106, 117, 120, and 131). Among these, mutants R75A, Y11A, V42A, N43A, T46A, and Y47A exhibited varying degrees of reduction in sfGFP/OD_{600} values across different L-carnitine concentrations. In contrast, mutations S93A, K40A, E96A, K97A, R102A, R131A enhanced output signal intensity in response to L-carnitine at 10^{-1} mM. The normalized fluorescence signals of the Y11A, V42A, N43A, T46A and Y47A mutants decreased about 80 %, when the concentration of L-carnitine was 10^{-3} mM, the sfGFP/OD_{600} value of the control sensor was 1704 ± 22, while the sfGFP/OD_{600} value for the mutants ranged from 312 ± 24 to 363 ± 11. Which indicating that the mutation of R75, Y11, V42, N43, T46 and Y47 to alanine may change the binding pocket of the CaiF protein, which affected the binding with L-carnitine (Fig. 4a).

Notably, the R75A mutation resulted in an almost complete loss of downstream DNA transcriptional expression. Structural analysis revealed that residue R75 not only forms effective electrostatic and hydrogen bond interactions with DNA but also establishes a hydrogen bond network with residue T46, which is crucial for maintaining the protein's structural stability. Molecular dynamics simulations revealed that the R75A mutation not only decreased the binding affinity by 40 kcal/mol (from −169 kcal/mol in WT to −129 kcal/mol in R75A), but also resulted in increased structural fluctuations throughout the protein, with particularly elevated amplitudes in residues 66–80 (Fig. 4b and c) (Fig. S1). This destabilization of key interactions likely accounts for the observed reduction in fluorescence intensity following the R75A mutation. Taken together, the R75A mutation demonstrated this region as a critical domain for DNA recognition and binding. This finding guided the subsequent engineering strategy toward fine-tuning the binding affinity within this region rather than disrupting it completely. Such understanding formed the foundation for rational modification to expand the biosensor's detection range while maintaining its fundamental functionality.

3.3. *Extension the dynamic range of the L-carnitine biosensor*

Based on the key sites identified by alanine scanning (Y11, V42, N43, T46, Y47, R75), we performed substitutions of the selected amino acids with residues of similar side-chain volume within each category

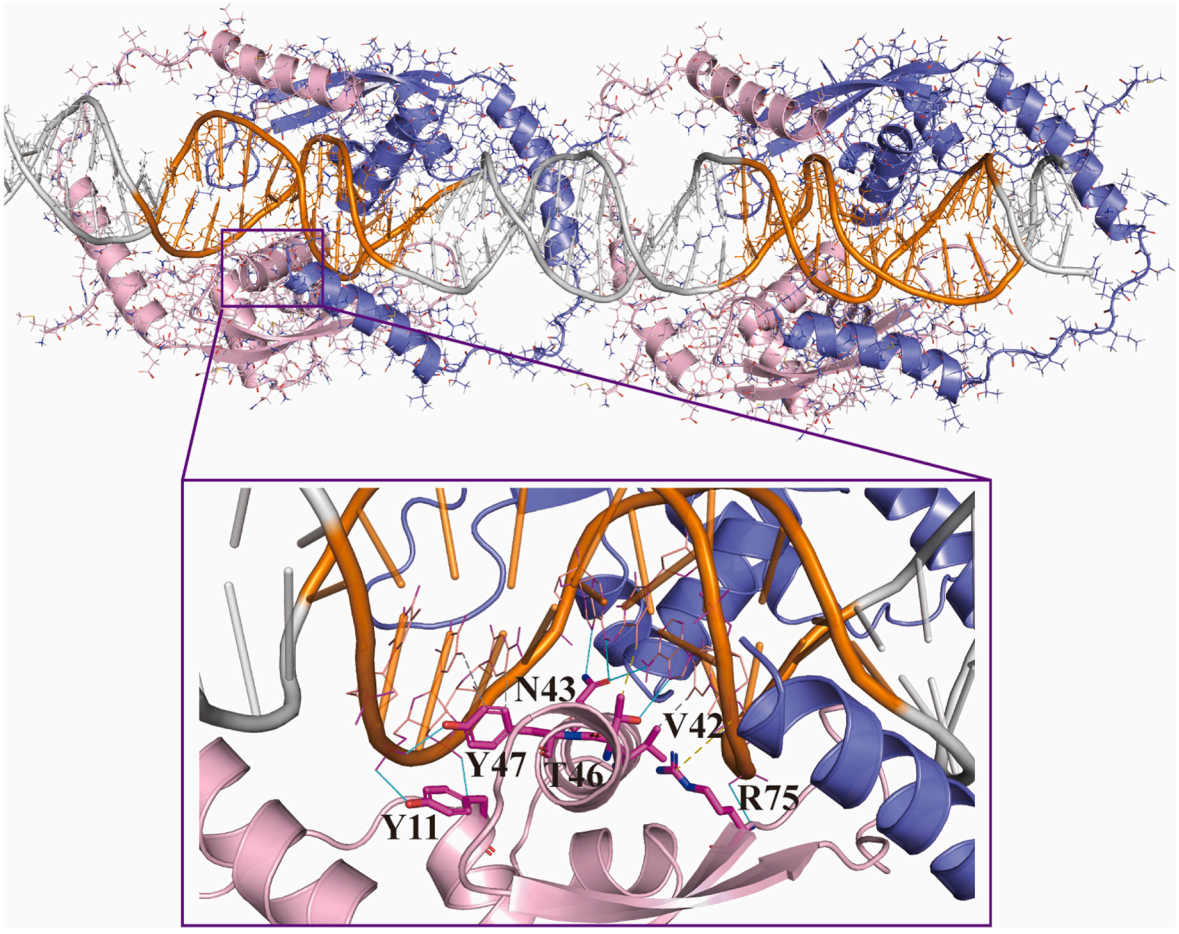

Fig. 3. Predicted structure of the CaiF-DNA complex. The three-dimensional structure of CaiF transcription factor bound to its target DNA sequence was modeled using the AlphaFold3 Server [27]. Among them, pink and purple are two reverse complementary sequences in the binding domain, 5′-CAATATTGAAA-3′ and 5′-TTTCAATATTG-3′, respectively, which are also the target sites of CaiF, so each DNA segment may require two CaiF binding. The key binding regions and residues are shown in the magnified view. Hydrogen bond interactions, hydrophobic interactions, and salt bridges are represented by blue solid lines, gray dashed lines, and yellow dashed lines, respectively. The DNA are shown in gray and the binding domain was bright orange. The residues are shown in magenta sticks.

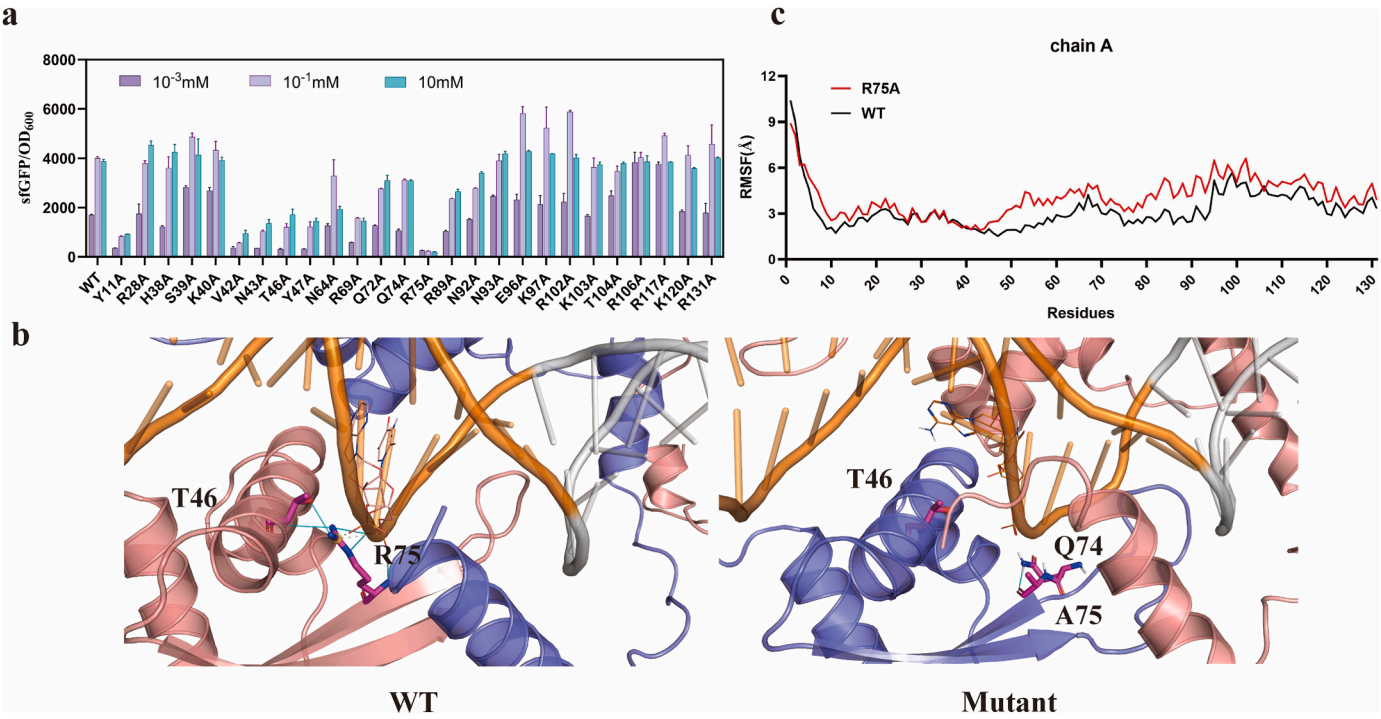

Fig. 4. Interchain mutation analysis of CaiF. (a) The relationship between sensor mutants and concentration response. (b) Comparison of interaction networks before and after R75A mutation. Hydrogen bond and hydrophobic interactions are depicted by blue solid lines and yellow dashed lines, respectively. The DNA are shown in gray and the binding domain was bright orange, while residues are highlighted in magenta. (c) Root Mean Square Fluctuation (RMSF) analysis comparing residue dynamics in chain A before and after R75A mutation.

(hydrophobic, polar, negatively charged, and positively charged). This functional diversity-oriented volume-conservative substitution strategy ensures comprehensive substitutions, including both conservative and non-conservative replacements, thereby minimizing structural perturbations while maximizing the exploration of functional diversity. Among them, Y11L exhibited differences in response values between 1 and 100 mM, with these values increasing as the concentration increased. In contrast, Y47W showed saturation at 1 mM; however, its output fluorescence signal intensity was significantly higher than that of the wild-type biosensor. Therefore, two advantageous mutants Y11L, and Y47W were successfully obtained (Fig. 5a–f). To further explore the specific response ranges of these advantageous mutants, exogenous L-carnitine was added at concentrations ranging from 10^{-6} mM–10 mM for evaluation. Among them, Y47W showed significant advantages in both fluorescence intensities and concentration response range, with the maximum fluorescence intensities reached 8000, which is double that of the control, and a response range of 10^{-4} mM to 10^{-1} mM. The mutant Y11L does not show an advantage in fluorescence intensity but significantly expands the concentration response range to between 10^{-3} mM and 1 mM (Fig. 5g).

3.4. Development of the mutants with high outputs and wider detection ranges

Output signal and response range are key performance indicators of biosensors. Although Y11L and Y47W exhibited enhanced concentration response ranges, their output signals did not meet expectations. Therefore, we selected the mutants (R89A, N92A, N93A, E96A, K97A, R102A, K103A, T104A, R106A, R117, K120) for further combination and mutagenesis studies. These residues do not directly participate in the specific DNA recognition region but may contribute to protein stability and nonspecific DNA binding. Such interactions could influence the biosensor's output values and extend its detection range (Fig. S2). A total of 22 combinatorial mutants were successfully generated through site-directed mutagenesis. Compared with the mutant combinations on Y47W, the mutant combinations on Y11L generally exhibited lower output fluorescence signals. Among them, the superposition of the N92A mutation had a positive impact on both Y11L and Y47W, resulting in enhanced response ranges and improved output signals (Fig. 6a).

The combined mutants Y11L/N92A, Y11L/N93A, Y11L/R106A and Y11L/R117A exhibited a significant increase in fluorescence output (Fig. 6a). Upon optimization of the exogenous concentration, the detection range of the Y11L/N92A mutant was successfully extended to 10^{-4} mM–10 mM. At a concentration of 10 mM, the sfGFP/OD_{600} value reached 9126, representing a 5.5-fold increase in fluorescence intensity compared to the Y11L mutant and a 2.7-fold increase compared to the wild-type biosensor. Another notable combination mutant, Y11L/R106A, demonstrated a substantially expanded response range of 10^{-3} mM–30 mM. Although its fluorescence output was slightly lower than that of Y11L/N92A, the sfGFP/OD_{600} value still increased to 6201 at 10 mM concentration (Fig. 6b).

The mutant combinations Y47W/R89A, Y47W/N92A, Y47W/K97A, and Y47W/R102A derived from the Y47W were selected for detailed concentration analysis due to their superior performance (Fig. 6a). These mutants exhibited enhanced fluorescence output and extended detection ranges. Notably, Y47W/R89A showed significant improvements, with its concentration response range expanded to 10^{-4} mM–10 mM. This represents a 1000-fold increase in detection range compared to the wild-type biosensor. The output fluorescence signal intensity was also markedly enhanced. Upon exogenous addition of 10 mM L-carnitine, the sfGFP/OD_{600} value of Y47W/R89A reached 10970, representing a 2-fold increase compared to the Y47W mutant and a 3.3-fold increase relative to the wild-type biosensor (Fig. 6c).

Obviously, the mutation combination of R89A has a significant improvement on the performance of the biosensor at the Y47W site. Similarly, the mutant combination Y11L/N92A at the Y11L site has demonstrated a notable increase in fluorescence signal output and an expanded detection range. These improvements render these mutants

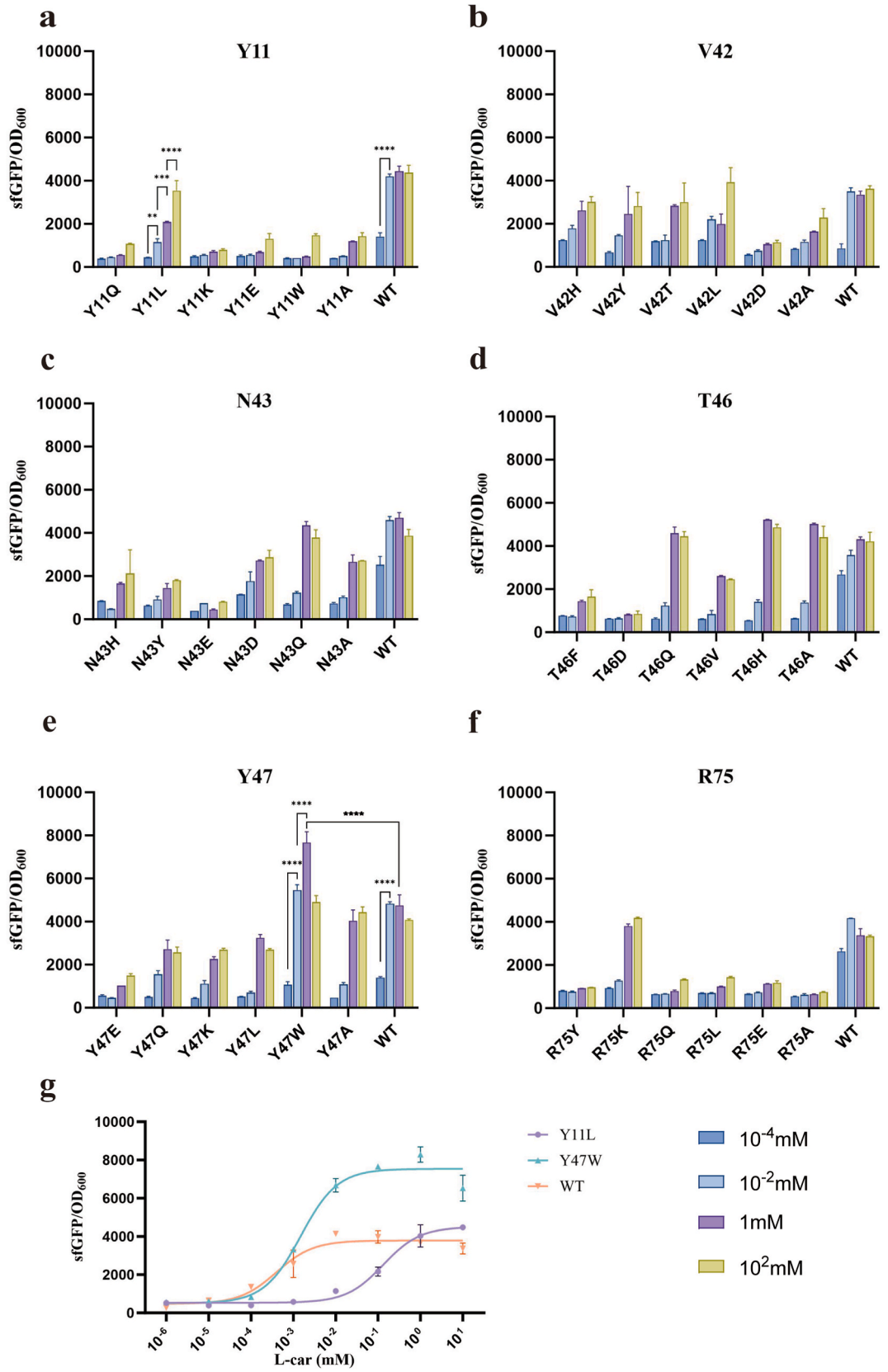

Fig. 5. Site-directed mutagenesis of CaiF was performed to obtain mutants with expanded response range. (a–f) The response range of the mutants (Y11, V42, N43, T46, Y47, R75) was evaluated after exogenous addition of L-carnitine concentrations of 10^{-4} mM, 10^{-2} mM, 1 mM and 10^{2} mM. (g) Dose-response curves to exogenous L-carnitine for mutants with expanded response range in *E. coli* BW25113 (DE3) Δ*caiA* cultivated. The fluorescence was determined at each indicated effector concentration and normalized to the cell density. The curves were fitted to the Hill equation. The maximum normalized fluorescence signal observed during the cultivation process is shown. Error bars indicate the standard deviation of the mean of three replicates.

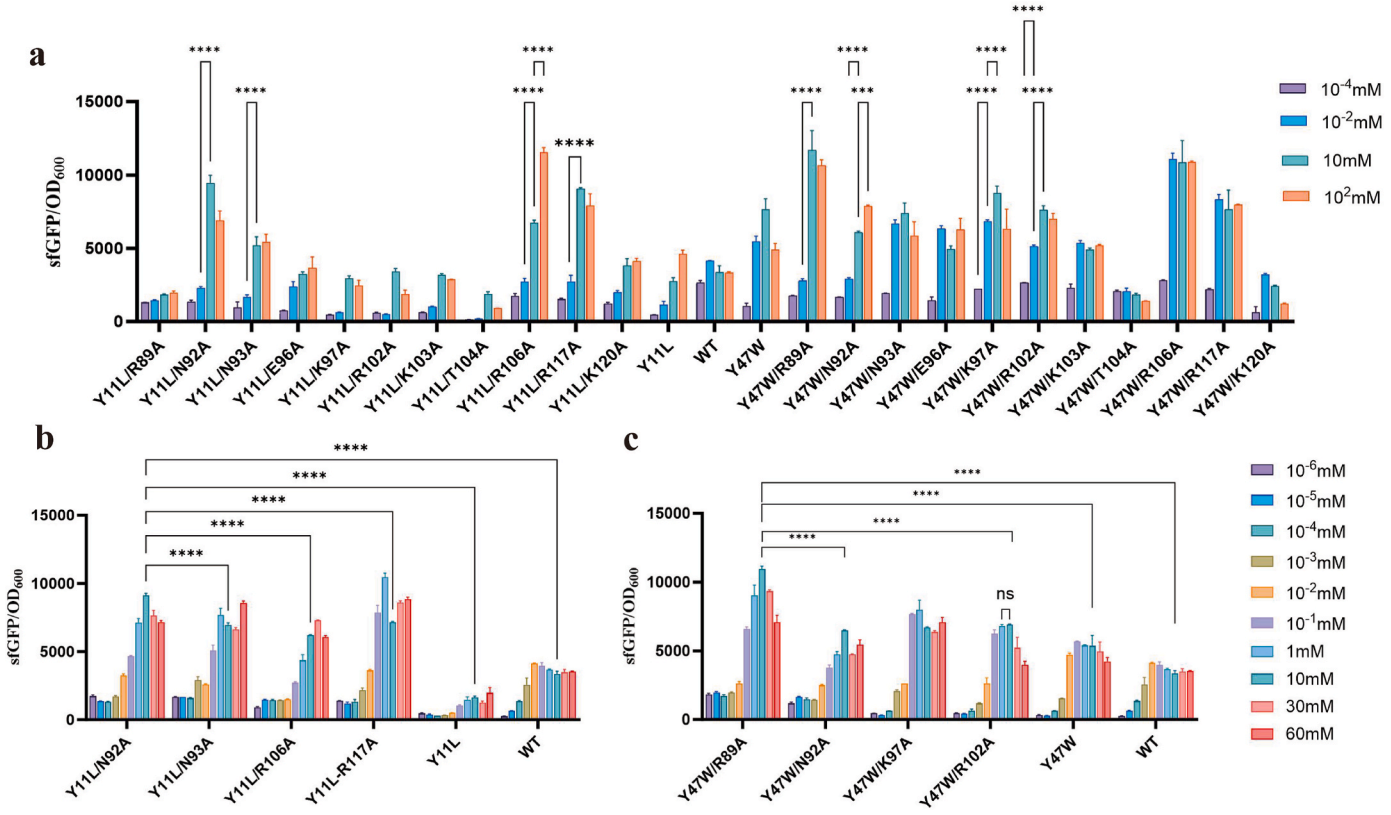

Fig. 6. Comparison of combinatorial mutant Y11L and Y47W. (a) The response values of wild type and mutants towards 10^{-4} mM, 10^{-2} mM, 10 mM and 10^{2} mM L-carnitine (b) The mutant obtained by superimposing alanine on the basis of Y11L. The response range of the mutant was evaluated after exogenous addition of L-carnitine concentrations of 10^{-6} mM–60 mM. (c) The mutant obtained by superimposing alanine on the basis of Y47W. The response range of the mutant was evaluated after exogenous addition of L-carnitine concentrations of 10^{-6} mM–60 mM. The maximum normalized fluorescence signal observed during the cultivation process is shown. Error bars indicate the standard deviation of the mean of three replicates.

more promising for biosensor applications, allowing for more efficient detection and response to target molecules.

4. Conclusion

The core principle of a transcription factor-based biosensor is to exploit the specific recognition and binding capacity of transcription factors to particular signal molecules, thereby regulating the expression of downstream genes and enabling the detection of target molecules. Subsequently, a biosensor with superior performance can be derived from its key components. The first component is the transcription factor itself, which can be engineered via directed evolution technology to enhance or diminish its binding affinity to the target molecule [34,35]. Additionally, research has been conducted on fusing transcription factors with other functional proteins to amplify signal output [36]. The second key component is the promoter, which can be engineered by modifying its sequence and structure to optimize the expression level of the transcription factor [21]. The signal amplification element is another aspect that warrants attention. By incorporating specific genetic circuits, the performance of the biosensor can be optimized through the use of positive feedback mechanisms or multi-layered signal amplification pathways.

In this study, we constructed a biosensor in BW25113 (DE3) Δ*caiA* with the substrate response range was 10^{-4} mM-10^{-2} mM. The DNA binding site of CaiF was predicted by structural prediction and model construction of the CaiF-DNA complex using AlphaFold3, and was verified by alanine scanning mutagenesis. The biosensor based on R75A could hardly respond to L-carnitine, mutants Y11A, V42A, N43A, T46A, Y47A exhibited low sensitivity and slow response to L-carnitine, which confirmed the credibility of our previously constructed model. Although alanine scanning provides great convenience for finding the recognition of key amino acid residues and DNA binding sites in CaiF, the protein structure of CaiF still needs to be determined by further experiments, such as X-ray crystals, Cryo-EM, etc.

A functional diversity-oriented substitution strategy with similar side-chain volumes was applied to six residues in the target protein. Two mutants (Y11L and Y47W) exhibited significantly improved response ranges. Subsequently, based on the Y11L and Y47W mutants and guided by the results of alanine scanning, we performed combinatorial mutagenesis targeting key sites associated with increased fluorescence signals, ultimately obtained the optimal mutant Y47W/R89A. The mutant demonstrated a 1000-fold expansion in its concentration detection range compared to the control biosensor, surpassing the dynamic range of the reported biosensor by Pierre Kugler et al. by two orders of magnitude (100-fold), while simultaneously achieving a 3.3-fold amplification in its output signal intensity [12]. The biosensor constructed based on the CaiF mutant $CaiF^{Y47W/R89A}$ has a concentration response range of 10^{-4} mM–10 mM, which is significantly superior to the wild type, making it more advantageous for screening strains that overproduce L-carnitine.

This study has obtained a biosensor with a significantly expanded detection range, and the in-depth investigation of the structure and mechanism of CaiF has provides valuable insights and rational engineering strategies for optimizing its performance. And provides some valuable information for further analysis of the functional domain of CaiF. Based on the directed evolution strategy of computer-aided design and structure-guided biosensors, researchers can significantly reduce the inherent blindness of the traditional "design-build-test" cycle. By integrating advanced mathematical models, machine learning algorithms, and deep learning frameworks, researchers can rationally predict the binding conformational changes between transcription factors

and ligands, and optimize the synergy of regulatory elements (such as promoter strength and ribosome binding site design, etc.). This holistic approach enables the systematic enhancement of biosensor sensitivity, dynamic detection range, and specificity, thereby substantially improving their overall performance [37–39].

However, this field still faces numerous challenges. Insufficient structural analysis of transcription factors can limit the accuracy of computer simulations in predicting functional changes [40]. Furthermore, the rational and robust design of a large number of component libraries may be limited by the system, and the evolution direction of the components cannot be completely controlled [41–44]. Moreover, the utilization of model training necessitates substantial data support and rigorous experimental validation. While these factors can be refined through consultation of existing literature or rational modeling approaches, future endeavors should focus on the development of more finely-tuned biosensors to achieve precise detection of metabolite concentrations.

CRediT authorship contribution statement

Tingting Li: Writing – review & editing, Writing – original draft, Visualization, Validation, Methodology, Investigation, Formal analysis, Data curation. **Huina Dong:** Writing – review & editing, Validation, Resources, Project administration, Methodology, Funding acquisition. **Jinlong Li:** Writing – review & editing, Validation, Software, Project administration, Methodology. **Huiying Wang:** Validation, Methodology, Investigation. **Chunxiang Pu:** Visualization, Validation, Software. **Siyu Chen:** Visualization, Validation. **Zhiying Yang:** Validation, Data curation. **Xinyi Ren:** Visualization, Validation. **Xuan Liu:** Visualization, Validation. **Zhaoxia Jin:** Writing – review & editing, Validation, Project administration, Funding acquisition. **Dawei Zhang:** Writing – review & editing, Project administration, Funding acquisition.

Declaration of competing interest

The authors declare that they have no known competing financial interests or personal relationships that could have appeared to influence the work reported in this paper.

Acknowledgments

This work was supported by the National Key R&D Program of China (2022YFC2106100), the National Science Fund for Distinguished Young Scholars (22325807), the National Natural Science Foundation of China (22178372, 32300069, 42177112), and the International Partnership Program of the Chinese Academy of Sciences (306GJHZ2023019GC).

Appendix A. Supplementary data

Supplementary data to this article can be found online at https://doi.org/10.1016/j.synbio.2025.04.012.

References

[1] Franken J, Burger A, Swiegers JH, et al. Reconstruction of the carnitine biosynthesis pathway from *Neurospora crassa* in the yeast *Saccharomyces cerevisiae*. Appl Microbiol Biotechnol 2015;99(15):6377–89. https://doi.org/10.1007/s00253-015-6561-x.
[2] Reuter SE, Evans AM. Carnitine and acylcarnitines: pharmacokinetic, pharmacological and clinical aspects. Clin Pharmacokinet 2012;51(9):553–72. https://doi.org/10.1007/BF03261931.
[3] Bernal V, Arense P, Cánovas M, Biopigments, et al. l-Carnitine, the vitamin BT: uses and production by the secondary metabolism of bacteria. Industrial Biotechnology of Vitamins, Biopigments, and Antioxidants. Wiley-VCH; 2016. p. 389–419.
[4] Vaz FM, Wanders RJ. Carnitine biosynthesis in mammals. Biochem J 2002;361(3):417–29. https://doi.org/10.1042/0264–6021:3610417.
[5] Winter SC. Treatment of carnitine deficiency. J Inherit Metab Dis 2003;26(2–3):171–80. https://doi.org/10.1023/a:1024433100257.
[6] Johri AM, Heyland DK, Hétu MF, et al. Carnitine therapy for the treatment of metabolic syndrome and cardiovascular disease: evidence and controversies. Nutr Metab Cardiovasc Dis 2014;24(8):808–14. https://doi.org/10.1016/j.numecd.2014.03.007.
[7] Kugler P, Trumm M, Frese M, et al. L-carnitine production through biosensor-guided construction of the *Neurospora crassa* biosynthesis pathway in *Escherichia coli*. Front Bioeng Biotechnol 2021:9. https://doi.org/10.3389/fbioe.2021.671321.
[8] Eichler K, Buchet A, Lemke R, et al. Identification and characterization of the *caiF* gene encoding a potential transcriptional activator of carnitine metabolism in *Escherichia coli*. J Bacteriol 1996;178(5):1248–57. https://doi.org/10.1128/jb.178.5.1248-1257.1996.
[9] Buchet A, Nasser W, Eichler K, et al. Positive co-regulation of the *Escherichia coli* carnitine pathway *cai* and *fix* operons by CRP and the CaiF activator. Mol Microbiol 2002;34(3):562–75. https://doi.org/10.1046/j.1365-2958.1999.01622.x.
[10] Eichler K, Bourgis F, Buchet A, et al. Molecular characterization of the cai operon necessary for carnitine metabolism in *Escherichia coli*. Mol Microbiol 1994;13(5):775–86. https://doi.org/10.1111/j.1365-2958.1994.tb00470.x.
[11] Eichler K, Buchet A, Bourgis F, et al. The *fix Escherichia coli* region contains four genes related to carnitine metabolism. J Basic Microbiol 1995;35(4):217–27. https://doi.org/10.1002/jobm.3620350404.
[12] Kugler P, Fröhlich D, Wendisch VF. Development of a biosensor for crotonobetaine-CoA ligase screening based on the elucidation of *Escherichia coli* carnitine metabolism. ACS Synth Biol 2020;9(9):2460–71. https://doi.org/10.1021/acssynbio.0c00234.
[13] Dabirian Y, Li X, Chen Y, et al. Expanding the dynamic range of a transcription factor-based biosensor in *Saccharomyces cerevisiae*. ACS Synth Biol 2019;8(9):1968–75. https://doi.org/10.1021/acssynbio.9b00144.
[14] Alvarez Gonzalez G, Chacón M, Butterfield T, et al. Tuning the performance of a TphR-based terephthalate biosensor with a design of experiments approach. Metab. Eng. Commun. 2024;19. https://doi.org/10.1016/j.mec.2024.e00250.
[15] Dacquay LC, McMillen DR. Improving the design of an oxidative stress sensing biosensor in yeast. FEMS Yeast Res 2021;21(4). https://doi.org/10.1093/femsyr/foab025.
[16] Lebovich M, Andrews LB. Surveying the genetic design space for transcription factor-based metabolite biosensors: synthetic gamma-Aminobutyric acid and Propionate biosensors in *E. coli* Nissle 1917. Front Bioeng Biotechnol 2022:10. https://doi.org/10.3389/fbioe.2022.938056.
[17] Lu M, Sha Y, Kumar V, et al. Transcription factor-based biosensor: a molecular-guided approach for advanced biofuel synthesis. Biotechnol Adv 2024;72. https://doi.org/10.1016/j.biotechadv.2024.108339.
[18] Fan C, He N, Yuan J. Cascaded amplifying circuit enables sensitive detection of fungal pathogens. Biosens Bioelectron 2024:250. https://doi.org/10.1016/j.bios.2024.116058.
[19] Angelici B, Mailand E, Haefliger B, et al. Synthetic Biology Platform for sensing and integrating endogenous transcriptional Inputs in Mammalian cells. Cell Rep 2016;16(9):2525–37. https://doi.org/10.1016/j.celrep.2016.07.061.
[20] Wu Y, Li Y, Jin K, et al. CRISPR–dCas12a-mediated genetic circuit cascades for multiplexed pathway optimization. Nat Chem Biol 2023;19(3):367–77. https://doi.org/10.1038/s41589-022-01230-0.
[21] Brandsen BM, Mattheisen JM, Noel T, et al. A biosensor strategy for *E. coli* based on ligand-dependent stabilization. ACS Synth Biol 2018;7(9):1990–9. https://doi.org/10.1021/acssynbio.8b00052.
[22] Teng Y, Gong X, Zhang J, et al. Investigating and engineering an 1,2-propanediol-responsive transcription factor-based biosensor. ACS Synth Biol 2024;13(7):2177–87. https://doi.org/10.1021/acssynbio.4c00237.
[23] Xiao D, Hu C, Xu X, et al. A d,l-lactate biosensor based on allosteric transcription factor LldR and amplified luminescent proximity homogeneous assay. Biosens Bioelectron 2022:211. https://doi.org/10.1016/j.bios.2022.114378.
[24] Kovach M, Elzer P, Hill D, et al. Four new derivatives of the broad-host-range cloning vector pBBR1MCS, carrying different antibiotic-resistance cassettes. Gene 1995;166(1):175–6. https://doi.org/10.1016/0378-1119(95)00584-1.
[25] Kovach M, Phillips R, Elzer P, et al. pBBR1MCS: a broad-host-range cloning vector. Biotechniques 1994;16:800–2.
[26] Zhao D, Yuan S, Xiong B, et al. Development of a fast and easy method for Escherichia coli genome editing with CRISPR/Cas9. Microb Cell Fact 2016;15(1). https://doi.org/10.1186/s12934-016-0605-5.
[27] Abramson J, Adler J, Dunger J, et al. Accurate structure prediction of biomolecular interactions with AlphaFold 3. Nature 2024;630(8016):493–500. https://doi.org/10.1038/s41586-024-07487-w.
[28] Case DA, Aktulga HM, Belfon K, et al. Amber 2022. San Francisco: University of California; 2022.
[29] Drobizhev M, Tillo S, Makarov NS, et al. Absolute two-photon absorption spectra and two-Photon brightness of orange and red fluorescent proteins. J Phys Chem B 2009;113(4):855–9. https://doi.org/10.1021/jp8087379.
[30] Zhang Y, Ptacin JL, Fischer EC, et al. A semi-synthetic organism that stores and retrieves increased genetic information. Nature 2017;551(7682):644–7. https://doi.org/10.1038/nature24659.
[31] Shaner NC, Campbell RE, Steinbach PA, et al. Improved monomeric red, orange and yellow fluorescent proteins derived from Discosoma sp. red fluorescent protein. Nat Biotechnol 2004;22(12):1567–72. https://doi.org/10.1038/nbt1037.
[32] Li L, Martinez SS, Hu W, et al. A specific E3 ligase/deubiquitinase pair modulates TBP protein levels during muscle differentiation. Elife 2015;4:e08536. https://doi.org/10.7554/eLife.08536.
[33] Pédelacq J-D, Cabantous S, Tran T, et al. Engineering and characterization of a superfolder green fluorescent protein. Nat Biotechnol 2006;24(1):79–88. https://doi.org/10.1038/nbt1172.

[34] Ferreira SS, Antunes MS. Re-Engineering plant phenylpropanoid metabolism with the aid of synthetic biosensors. Front Plant Sci 2021;12. https://doi.org/10.3389/fpls.2021.701385.
[35] Zhou GJ, Zhang F. Applications and tuning strategies for transcription factor-based metabolite biosensors. Biosensors 2023;13(4). https://doi.org/10.3390/bios13040428.
[36] Younger AKD, Su PY, Shepard AJ, et al. Development of novel metabolite-responsive transcription factors via transposon-mediated protein fusion. Protein Eng Des Sel 2018;31(2):55–63. https://doi.org/10.1093/protein/gzy001.
[37] Guo J, Wang T, Guan C, et al. Improved sgRNA design in bacteria via genome-wide activity profiling. Nucleic Acids Res 2018;46(14):7052–69. https://doi.org/10.1093/nar/gky572.
[38] Ding N, Yuan Z, Zhang X, et al. Programmable cross-ribosome-binding sites to fine-tune the dynamic range of transcription factor-based biosensor. Nucleic Acids Res 2020;48(18):10602–13. https://doi.org/10.1093/nar/gkaa786.
[39] Liu X, Gupta STP, Bhimsaria D, et al. De novo design of programmable inducible promoters. Nucleic Acids Res 2019;47(19):10452–63. https://doi.org/10.1093/nar/gkz772.
[40] De Las Heras A, Carreño CA, Martínez-García E, et al. Engineering input/output nodes in prokaryotic regulatory circuits. FEMS Microbiol Rev 2010;34(5):842–65. https://doi.org/10.1111/j.1574-6976.2010.00238.x.
[41] Wan X, Volpetti F, Petrova E, et al. Cascaded amplifying circuits enable ultrasensitive cellular sensors for toxic metals. Nat Chem Biol 2019;15(5):540–8. https://doi.org/10.1038/s41589-019-0244-3.
[42] Wang T, Guan C, Guo J, et al. Pooled CRISPR interference screening enables genome-scale functional genomics study in bacteria with superior performance. Nat Commun 2018;9(1). https://doi.org/10.1038/s41467-018-04899-x.
[43] Kim HK, Min S, Song M, et al. Deep learning improves prediction of CRISPR–Cpf1 guide RNA activity. Nat Biotechnol 2018;36(3):239–41. https://doi.org/10.1038/nbt.4061.
[44] Kimura Y, Kawai-Noma S, Saito K, et al. Directed evolution of the stringency of the LuxR *Vibrio fischeri* quorum sensor without OFF-state selection. ACS Synth Biol 2020;9(3):567–75. https://doi.org/10.1021/acssynbio.9b00444.